SCIENTIFIC REPORTS
nature research

OPEN

Non-proliferative neurogenesis in human periodontal ligament stem cells

Carlos Bueno[1*], Marta Martínez-Morga[2] & Salvador Martínez[1]

Understanding the sequence of events from undifferentiated stem cells to neuron is not only important for the basic knowledge of stem cell biology, but also for therapeutic applications. In this study we examined the sequence of biological events during neural differentiation of human periodontal ligament stem cells (hPDLSCs). Here, we show that hPDLSCs-derived neural-like cells display a sequence of morphologic development highly similar to those reported before in primary neuronal cultures derived from rodent brains. We observed that cell proliferation is not present through neurogenesis from hPDLSCs. Futhermore, we may have discovered micronuclei movement and transient cell nuclei lobulation coincident to *in vitro* neurogenesis. Morphological analysis also reveals that neurogenic niches in the adult mouse brain contain cells with nuclear shapes highly similar to those observed during *in vitro* neurogenesis from hPDLSCs. Our results provide additional evidence that it is possible to differentiate hPDLSCs to neuron-like cells and suggest the possibility that the sequence of events from stem cell to neuron does not necessarily requires cell division from stem cell.

Neurons are highly polarized cells exhibiting functionally and structurally distinct processes called axons and dendrites[1,2]. Understanding the mechanisms that underlie the temporal and spatial control of neuronal polarization is not only important for neurobiology[3], but also for nerve regeneration in injured nervous systems[4].

The process of neuronal polarization has been studied for decades using dissociated rodent postnatal cerebellar granule neurons and embryonic hippocampal pyramidal neurons in culture[1,2]. The establishment of polarity in cultured rodent neurons are divided into different stages[5,6].

Upon isolation, dissociated pyramidal neurons retract their processes, so their neuronal development *in vitro* start as rounded spheres that spread lamellipodia (stage 1). These spheres appear symmetrical, extending and retracting several immature neurites of a similar length (stage 2). Elongation of a single process, that which presumably becomes the axon, breaks this symmetry (stage 3). The next step involves the remaining short neurites morphologically developing into dendrites (stage 4). The last step (stage 5) in neuronal polarization from dissociated pyramidal neurons in culture is the functional polarization of axon and dendrites, including dendritic spine formation and axon branch formation[5]. Dissociated granule neurons also present a lamellipodia after attaching to the substratum (stage 1). These spheres extend a unipolar process at a single site on the plasma membrane (stage 2) followed by extension of a second process from the opposite side of the cell body, resulting in a bipolar morphology (stage 3). One of the two axon elongates futher and start branching (stage 4), and shorter dendritic processes develop around the cell body (stage 5)[6].

Although much progress has been made in the knowledge of how rodent neurons establish their polarity[1–3,5,6], less is known about the process of neuronal polarization in human cells[7,8].

The major barrier to studying human neurons is the inaccessibility of living tissue, therefore an enormous effort has been made in this study to derive neurons from human stem cells[9–11].

Neural crest stem cells (NCSCs) are a migratory cell population that generate numerous cell lineages during development, including neurons and glia[12,13]. NCSCs can be isolated not only from embryonic neural crest, but also from fetal and adult neural crest-derived tissues[14].

The periodontal ligament (PDL) is a connective tissue surrounding the tooth root that contains a source of human NCSCs which can be accessed with minimal technical requirements and little inconvenience to the donor[15]. Isolation and characterization of multipotent stem cells from the human PDL have been previously described[16,17].

[1]Instituto de Neurociencias de Alicante (UMH-CSIC), San Juan, Alicante, 03550, Spain. [2]Department of Human Anatomy and Institute of Biomedical Research (IMIB), University of Murcia, Faculty of Medicine, Murcia, 30800, Spain. *email: cbueno@umh.es

In previous publication[18], we showed that human adult periodontal ligament (hPDL) tissue and hPDL-derived cells express marker genes of stem cells and neural crest cells. *In vitro*, hPDL-derived cells differentiate into neural-like cells based on cellular morphology and neural marker expression. *In vivo*, hPDL-derived cells survive, migrate and expressed neural markers after being grafted to the adult mouse brain. Futhermore, some hPDL-derived cells graft into neural stem cell (NSC) niches such as the ventricular-subventricular zone (V-SVZ) of the anterolateral ventricle wall and the subgranular zone (SGZ) of the dentate gyrus in the hippocampus. It is important to mention that the hPDLSCs located in the NSC niches show neural stem morphology.

Moreover, hPDLSCs expressed ion channel receptors[19] and displayed inward currents conducted through voltage-gated sodium (Na+) channels and spontaneous electrical activities after neurogenic differentiation[20,21]. Therefore, the neural crest origin[14,15] and neural differentiation potential both *in vitro* and *in vivo*[13–24], make human periodontal ligament stem cells (hPDLSCs) interesting for investigating stem cell to neuron differentiation mechanisms.

Here, we show that hPDLSCs-derived neural-like cells display a sequence of morphologic development highly similar to those reported before in primary neuronal cultures derived from rodent brains during neurogenesis, providing additional evidence that it is possible to differentiate hPDLSCs to neuron-like cells.

We observed that cell proliferation is not present through neurogenesis from hPDLSCs. In fact, the cell shape of hPDLSCs is reset and start their neuronal development as round spheres. Futhermore we may have discovered a transient cell nuclei lobulation coincident to *in vitro* neurogenesis, without being related to cell proliferation. We observed that small DNA containing structures may move within the cell to specific directions and temporarily form lobed nuclei.

Morphological analysis also reveals that the V-SVZ of the anterolateral ventricle wall and the SGZ of the hippocampal dentate gyrus in the adult mouse brain contains cells with nuclear shapes highly similar to those observed during *in vitro* neurogenesis from hPDLSCs. We suggest the possibility that neuronal differentiation from NSCs may also occur during *in vivo* adult mammalian neurogenesis without being related to cell proliferation.

Results

hPDLSCs cultured in basal media. Under proliferation conditions, hPDLSCs displayed a fibroblast-like morphology with low-density microvilli on the cell surface (Fig. 1a) and actin microfilaments and β-III tubulin microtubules oriented parallel to the longitudinal axis of the cell (Fig. 1b). The cytoskeletal protein class III beta-tubulin isotype is widely regarded as a neuronal marker in developmental neurobiology and stem cell research[25]. Dental and oral-derived stem cells displayed spontaneous expression of neural marker β-III tubulin, even without having been subjected to neural induction[26]. Western blot analysis verified the expression of β-III tubulin in hPDLSCs (Fig. 1c). During interphase, undifferentiated hPDLSCs displayed a flattened, ellipsoidal nucleus, often located in the center of the cell and with a nuclear volume around $925'356 \pm 52'6184\ \mu m^3$ (Fig. 1d).

During mitosis, β-III tubulin is present in the mitotic spindle and it is detectable in all phases of mitosis (Fig. 1e). The cytoskeletal protein class III beta-tubulin isotype is a component of the mitotic spindle in multiple cell types[27]. At the end of mitosis, division of the cytoplasm by cytokinesis is observed (Fig. 1f). Mitosis and cytokinesis last no more than 2 hours (Fig. 1g).

hPDLSCs cultured in neural induction media. After 14 days of neural differentiation conditions, the hPDLSCs displayed different morphologies, including round cells with small phase-bright cell bodies and short processes; highly irregulary-shaped cells; and, also, unipolar, bipolar and multipolar-shaped cells with small phase-bright cell bodies and multiple branched processes (Fig. 2a). In addition, cells of different size were also observed (Fig. 2b). Futhermore, microscopic analysis revealed that some hPDLSCs have different nuclear shapes, including lobed nuclei connected by an internuclear bridge (Fig. 2c).

We examined the sequence of developmental events during the first day in culture. We observed that different-shaped cells are stages of development of hPDLSCs during neural differentiation (Fig. 2d). The results may indicate that the cell culture simultaneously contains hPDLSCs at different stages of neurogenesis and neuronal polatization. We acknowledge that the definitive sequence of *in vitro* neurogenesis and neuronal polarization from hPDLSCs will be provided only by time-lapse microscopy of a single cell, but in our experimental conditions, several pieces of data suggest how these steps may occur.

***In vitro* neurogenesis from hPDLSCs.** After neural induction, hPDLSCs undergo a dramatic change in shape and size, first adopting highly irregular forms and then gradually contracting into round cells with small phase-bright cell bodies (Fig. 3a). Cytoskeletal remodeling is observed during the morphological changes that occurred when the hPDLSCs round up to a near-spherical shape. Actin microfilament not longer surround the nucleus and became cortical. Unlike actin, β-III tubulin seems to accumulate around the nucleus (Fig. 3b). Actin microfilament and β-III tubulin microtubule network are almost lost in the rounded cells (Fig. 3c).

Scanning electron micrographs show that hPDLSCs also experience dramatic changes in cell surface features. Under proliferation conditions, hPDLSCs remain very flat, presenting low-density microvilli on their surface (Fig. 1a), but there is a marked increase in the number of microvilli as the cells round up to near-spherical shape (Fig. 3d). We also observed that the surface of the rounded cells is almost devoid of microvilli (Fig. 3e).

These results are consistent with previous studies reporting that microvilli increase in number during mitosis but become greatly disminished in number after cytokinesis is completed and the cells enter interphase[28,29]. Our results may indicatate that the dramatic change in shape and size observed during neurogenesis from hPDLSCs is completed.

Morphological and immunocytochemical analysis revealed that rounded cells do not represent dividing cells due to the absence of cytokinesis, mitotic chromosomes and mitotic spindle during the described of *in vitro*

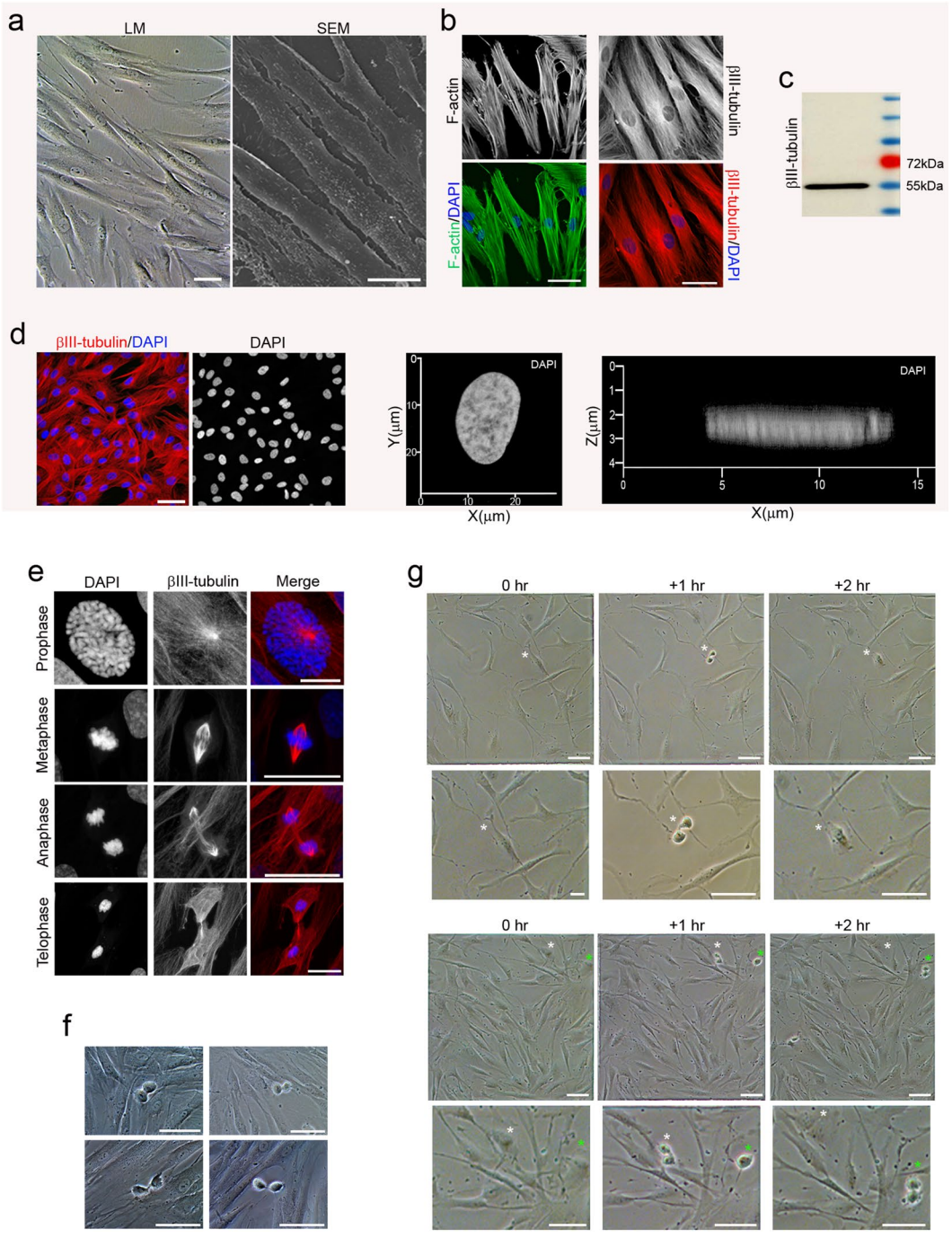

Figure 1. Morphology of hPDLSCs cultured in basal media. Undifferentiated hPDLSCs presented a fibroblast-like morphology with low-density microvilli on their surface (**a**) and actin microfilaments and β-III tubulin microtubules oriented parallel to the longitudinal axis of the cell (**b**). (**c**) Western blot analysis verified the expression of β-III tubulin. Protein size markers (in kilodaltons) are indicated on the side of the panel. (**d**) Undifferentiated hPDLSCs displayed a flattened, ellipsoidal nucleus often located in the center of the cell. (**e**) During mitosis, β-III tubulin is present in the mitotic spindle and it is detectable in all phases of mitosis. (**f**) At the end of mitosis, division of the cytoplasm by cytokinesis is observed. (**g**) Sequential images showing that mitosis and cytokinesis last no more than 2 hours. Scale bar: 25 μm. LM, light microscopy; SEM, scanning electron microscopy.

neurogenesis processes from hPDLSCs (Figs. 2, 3), contrary to what happens during mitosis (Fig. 1e–g). In addition, the duration of the morphological changes that occurred when the hPDLSCs round up to a near-spherical shape (Fig. 2d) last more than mitosis and cytokinesis (Fig. 1g).

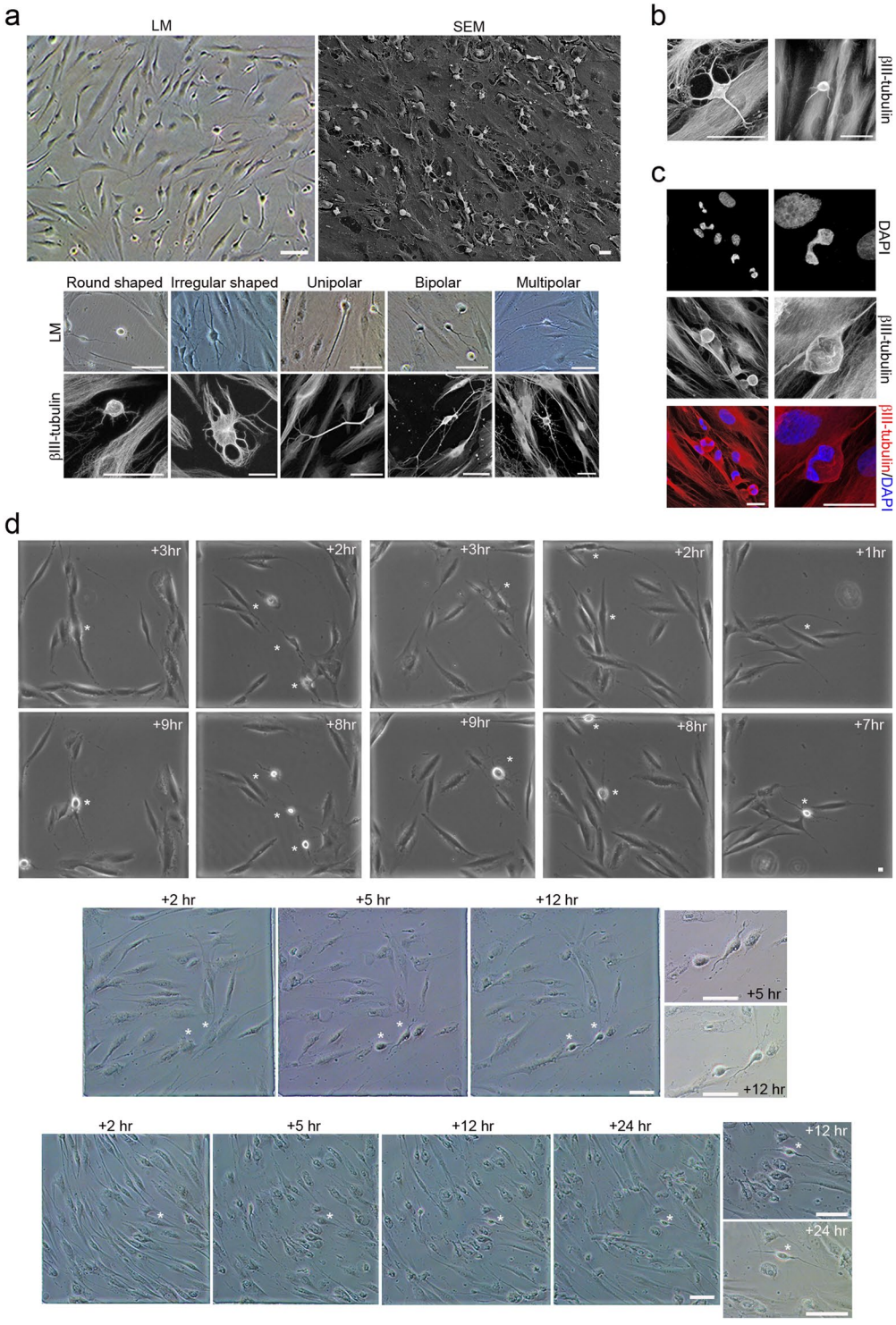

Figure 2. Morphological changes in hPDLSCs cultures during neural induction. (**a**) After 14 days of neural differentiation conditions, hPDLSCs with different morphologies were observed. (**b**) In addition, hPDLSCs of various size were also observed. (**c**) Microscopic analysis also revealed that some hPDLSCs have different nuclear size and shapes, including lobed nuclei connected by an internuclear bridge. (**d**) Sequential images showing that different-shaped cells are stages of development of hPDLSCs during neural differentiation. Scale bar: 25 μm. LM, light microscopy; SEM, scanning electron microscopy; +hr, hours post neural induction.

Neuronal polarization of hPDLSCs-derived neural-like cells. Morphological analysis revealed that hPDLSCs-derived neural-like cells display a sequence of morphologic development highly similar to those reported before in dissociated-cell cultures prepared from rodent brain[1,2,5,6] (Figs. 4–6). hPDLSCs-derived

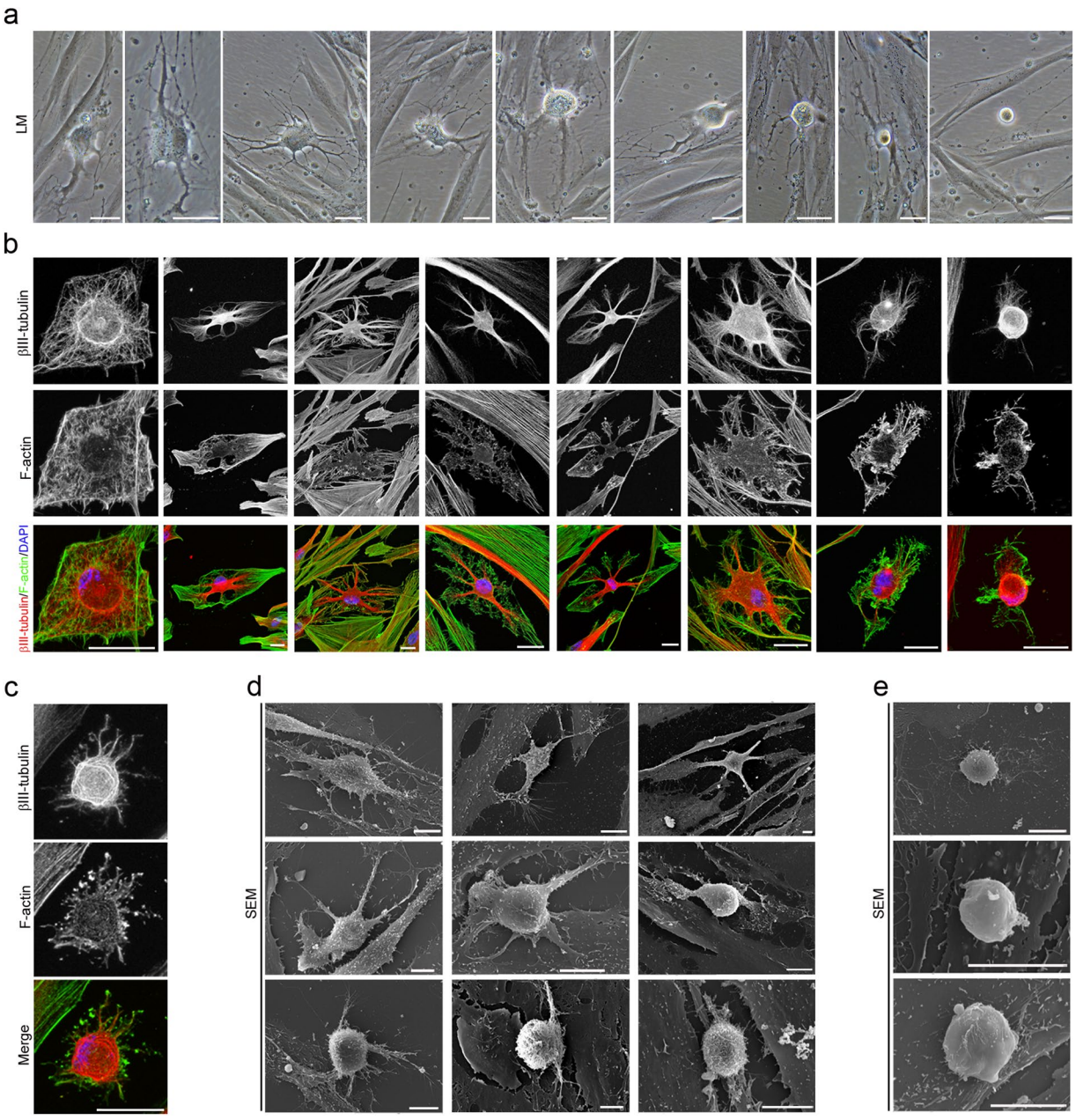

Figure 3. *In vitro* neurogenesis from hPDLSCs. (**a**) After neural induction, hPDLSCs undergo a shape and size change, adopting highly irregular forms first and then gradually contracting into round cells. (**b**) Cytoskeletal remodeling is observed during these morphological changes. Actin microfilament no longer surround the nucleus and become cortical. Unlike actin, β-III tubulin seems to accumulate around the nucleus. (**c**) the cytoskeletal network is almost lost in round cells. (**d**) Scanning electron micrographs show that there is a marked increase in the density of microvilli as the cells round up to near-spherical shape. (**e**) The surface of round cells is almost devoid of microvilli. The scale bars are 25 μm in the light microscope images, and 10 μm in the scanning electron micrographs. LM, light microscopy; SEM, scanning electron microscopy.

neural-like cells also start their development as rounded spheres that initiated neurite outgrowth at a single site on the plasma membrane[6], first becoming unipolar, stages 1–2 (Fig. 4a). We did not observe the development of lamellipodia around the circumference of the cell body. These unipolar cells, later transformed into cells containing several short neurites, developed around the cell body, stage 3 (Fig. 4b). An analysis of the cytoskeletal organization during spherical stages of hPDLSCs-derived neural-like cells showed that the β-III tubulin microtubules and actin microfilament network is reorganized. Cytoskeletal protein β-III tubulin was densely accumulated under the cellular membrane of the cell body and in cell neurites (Fig. 4a,b) while actin microfilaments were mainly found in cell neurites (Fig. 4c).

We observed that hPDLSCs-derived neural-like cells produce neurites that showed growth cone formations at their tips (Fig. 4c–e). The central domain of the growth cone contains β-III tubulin microtubules and the

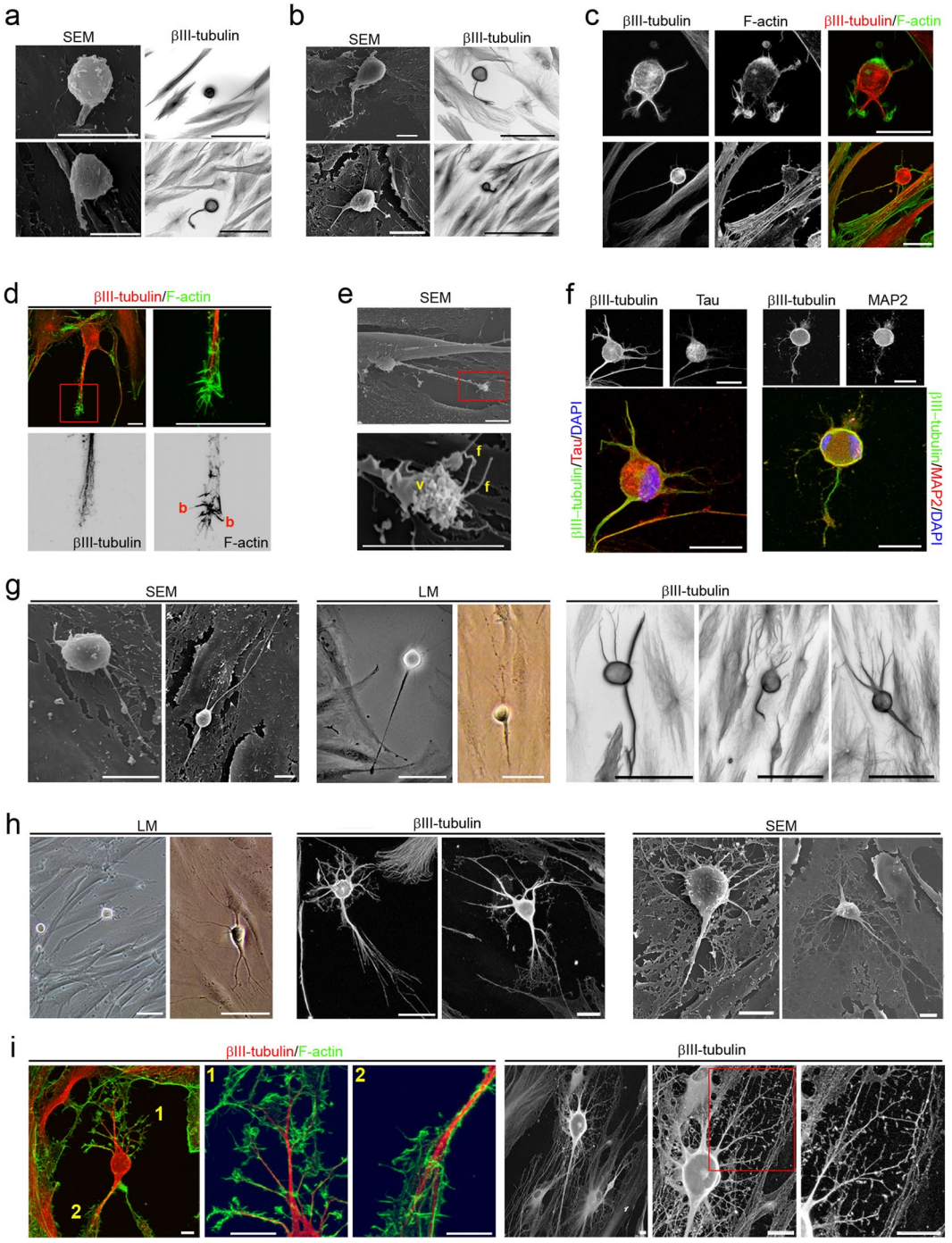

Figure 4. Neuronal polarization of hPDLSCs-derived neural-like cells. (**a**) hPDLSCs-derived neural-like cells start their development as rounded spheres that initiate neurite outgrowth at a single site on the plasma membrane. (**b**) These later transform into cells containing several short neurites developed around the cell body. (**c**) The cytoskeletal network is reorganizated. β-III tubulin accumulates densely under the cellular membrane of the cell body and in cell neurites while actin microfilaments are mainly found in cell neurites. (**d**) The peripheral domain in the growth cone of hPDLSCs-derived neural-like cells is composed of radial F-actin bundles and the central domain contains β-III tubulin microtubules. (**e**) Micrographs showing that the growth cone also contains filopodia and vesicles on the cell surface. (**f**) Microtubule-associated proteins Tau and MAP2 were also found in hPDLSCs-derived neural-like cells. At later stages of development, hPDLSCs-derived neural-like cells gradually adopt a complex morphology (**g**) giving rise to a variety of neuron-like forms (**h**). (**i**) Cytoskeletal protein β-III tubulin and F-actin staining shown that hPDLSCs-derived neural-like cells develop distinct axon-like and dendrite-like processes (numbers locate the areas shown in higher power). The scale bars are 25 μm in the light microscope images, and 10 μm in the scanning electron micrographs. b, actin bundles; f, filopodia; LM, light microscopy; SEM, scanning electron microscopy; v, vesicles.

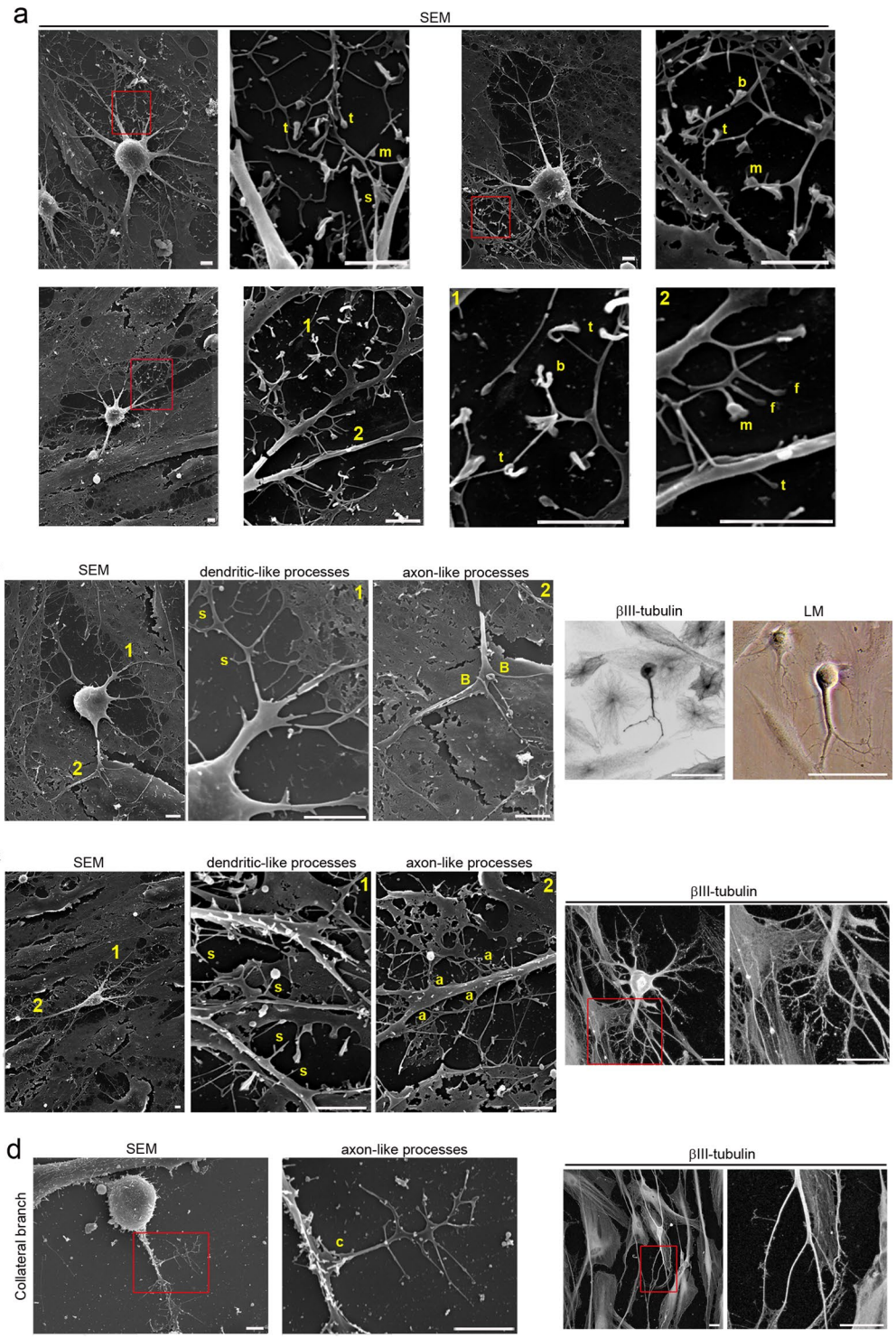

Figure 5. hPDLSCs-derived neural-like cells have developed well-differentiated axonal-like and dendritic-like domains. (**a**) Scanning electron micrographs show that hPDLSCs-derived neural-like cells are composed of multiple branched processes with different spine-like protusions highly similar to filopodium, mushroom, thin, stubby, and branched dendritic spines shapes. hPDLSCs-derived neural-like cells also display different types of axonal branch-like structures, including bifurcation (**b**), terminal arborization (**c**), and collateral formation (**d**) (inserts and numbers locate the areas showed in higher power). The scale bars are 25 μm in light microscope images and 5 μm in the scanning electron micrographs. a, arborization; B, bifurcation; b, branched; c, collateral formation; f, filopodium; LM, light microscopy; m, mushroom; S, spine-like protusions; s, stubby; SEM, scanning electron microscopy; t, thin.

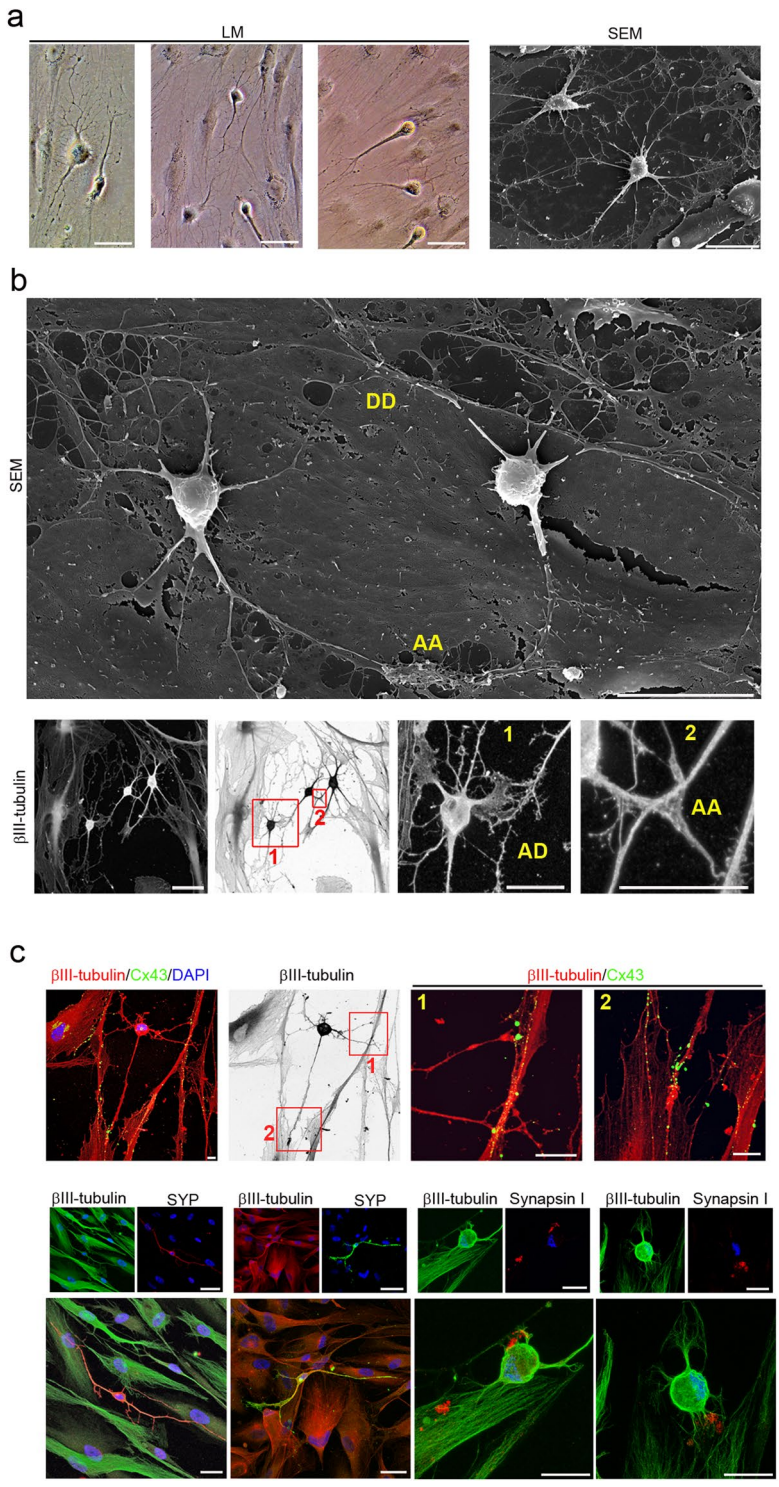

Figure 6. hPDLSCs-derived neural-like cells are connected by synapse-like interactions. hPDLSCs-derived neural-like cells connect to one another (**a**) through different types of synapses-like interactions, including dendrodendritic-like, axoaxonic-like and axodendritic-like synapses (**b**). (**c**) Synapse-associated proteins Cx43, Synaptophysin and Synapsin1 are found in the cell membrane of hPDLSCs-derived neural-like cells at the neurite contact areas. Scale bar: 25 μm. AA, axoaxonic-like synapse; AD, axodendritic-like synapse; DD, dendrodendritic-like synapse; LM, light microscopy; SEM, scanning electron microscopy.

peripheral domain is composed of radial F-actin bundles (Fig. 4d), similar to the typical spatial organization described in neurons[30,31]. Scanning electron micrographs also showed that the growth cone of hPDLSCs-derived neural-like cells contained filopodia and vesicles on the cell surface (Fig. 4e). These finding are consistent with a

previous study reporting that membrane addition and extension in growth cones is mediated by diverse mechanism, including exocytosis of vesicular components[32]. Microtubule-associated proteins Tau and MAP2 were also found in hPDLSCs-derived neural-like cells (Fig. 4f). At later stages of differentiation, the hPDLSCs-derived neural-like cells gradually adopted a complex morphology by forming several processes, stage 4 (Fig. 4g) that grew and arborized, adquiring dendritic-like and axonal-like identities, giving rise to a variety of neuron-like morphologies (Fig. 4h). The next step, stage 5, in neuronal polarization from rodent neurons in culture is the functional polarization of axon and dendrites, including dendritic spine formation and axon branch formation[1,2,5,6]. Dendritic spines are micron-sized dendrite membrane protrusions[33]. Depending on the relative sizes of the spine head and neck, they can be subdivided into different categories, including filopodium, mushroom, thin, stubby, and branched spines[34]. Dendritic spines are actin-rich compartments that protrude from the microtubule-rich dendritic shafts of principal neurons[35]. Based on morphology, complexity, and function, axon branching is grouped into different categories, including arborization, bifurcation, and collateral formation[36].

Our morphological analysis revealed that hPDLSCs-derived neural-like cells developed well-differentiated axonal-like and dendritic-like domains. These types of processes differ from each other in morphology (Figs. 4i and 5). Cytoskeletal protein β-III tubulin and F-actin staining showed that the hPDLSCs-derived neural-like cells comprised multiple branched dendrite-like processes with dendritic spines-like structures (Fig. 4i). Scanning electron micrographs showed that the hPDLSCs-derived neural-like cells also contained multiple branched dendrite-like processes with variously shaped spine-like protusions, highly similar to filopodium, mushroom, thin, stubby, and branched dendritic spines shapes (Fig. 5a). Futhermore, hPDLSCs-derived neural-like cells also displayed different types of axonal branch-like structures, including bifurcation (Fig. 5b), arborization (Fig. 5c), and collateral formation (Fig. 5d).

The last step in neuronal polarization from rodent neurons in culture is synapse formation[1,2,5,6]. The most frequent types of synaptic communication include axodendritic, axosomatic, axoaxonic and dendrodendritic synapses. Morphological analysis revealed that the hPDLSCs-derived neural-like cells connected to one another (Fig. 6a) through different types of synapse-like interactions, including dendrodendritic-like, axoaxonic-like and axodendritic-like synapses (Fig. 6b). Synapse-associated proteins Cx43, Synaptophysin and Synapsin1 were found accumulated in the cell surface of neurites (Fig. 6c).

Nuclear remodeling. Nuclear morphology was examined in hPDLSCs under proliferation and neural differentiation conditions. The dynamic localization of the nucleoli was analyzed by immunostaining for fibrillarin, the main component of the active transcription centers[37] and the dynamic localization of the nuclear lamina was analyzed by immunostaining for lamin A/C, a nuclear lamina component[38].

First, we analyzed the nuclear morphology in proliferative hPDLSCs. As noted above, during interphase, hPDLSCs displayed a flattened, ellipsoidal nucleus, often located in the center of the cell, and with a nuclear volume around $925.356 \pm 52.6184\,\mu m^3$ (Fig. 1d). The nuclei of hPDLSCs contained two or more nucleoli and the inside surface of the nuclear envelope is lined with the nuclear lamina (Fig. S1a). Previous studies have shown that the nuclear lamina and nucleolus are reversibly disassembled during mitosis[39,40]. Microscopic analysis of hPDLSCs revealed that the dynamic localization of fibrillarin and lamin A/C proteins during mitosis are similar to those observed in previous studies (Fig. S1b). Futhermore, β-III tubulin is present in the mitotic spindle and it is detectable in all phases of mitosis (Fig. S1b). In addition, mitotic chromosomes and cytokinesis were also observed (Figs. 1e–g and S1b).

Morphological analysis also revealed that nuclear remodeling occurred during *in vitro* neurogenesis from hPDLSCs (Fig. 7). We acknowledge that the definitive sequence of nuclear remodeling when hPDLSCs round up to near-spherical shape will only be provided by time-lapse microscopy, but our accumulated data suggests how these steps may occur.

Small DNA containing structures arise from the main nuclei (Fig. 7a) and start to move (Fig. 7b) towards specific positions within the cell (Fig. 7c) and temporarily form lobed nuclei (Fig. 7d). Later, these lobed nuclei connected to one another through small DNA containing structures (Fig. 7e) forming nucleoplasmic bridges (Fig. 7f). Finally, lobed nuclei connected by an internuclear bridge (Fig. 7g) join in a single nucleus with an eccentric position within hPDLSCs-derived neural-like cells (Fig. 7h).

These small DNA containing structures displayed a spherical or ovoid shape (Fig. S2a), and it seems that some of them are connected to the main body of the nucleus by thin strands of nuclear material (Fig. S2b). Fibrillarin and lamin A/C proteins were detected in these small DNA containing structures (Fig. S2c).

We also observed that the nuclear lamina (Fig. S3a) and nucleolus (Fig. S3b) are not disassembled during *in vitro* neurogenesis from hPDLSCs, contrary to what happens during mitosis[39,40]. Moreover, mitotic chromosomes, mitotic spindle and cytokinesis were not observed during the described of *in vitro* neurogenesis processes or neuronal polarization from hPDLSCs (Figs. 2–7 and S2–S5).

In addition, ultrastructural morphological characteristics of hPDLSCs were examined under neural differentiations conditions. Transmission electron microscopy (TEM) is considered the gold standard to confirm apoptosis[41]. Apoptotic cell contains certain ultrastructural morphological characteristics, including electron-dense nucleus, disorganized cytoplasmic organelles, large clear vacuoles, nuclear fragmentation and apoptotic bodies. TEM analysis revealed that hPDLSCs under neural differentiations conditions do not meet the criteria described above (Fig. S4). Therefore, hPDLSCs with lobed nuclei do not represent apoptotic cells.

During neuronal polarization, no lobed nuclei were observed as hPDLSCs-derived neural-like cells gradually acquired a more mature neuronal-like morphology (Fig. S5a). We also found that as the cells round up to a near-spherical shape the nuclear volume of the hPDLSCs decreases to an approximate volume of $279.589 \pm 38.8905\,\mu m^3$ (Fig. S5b).

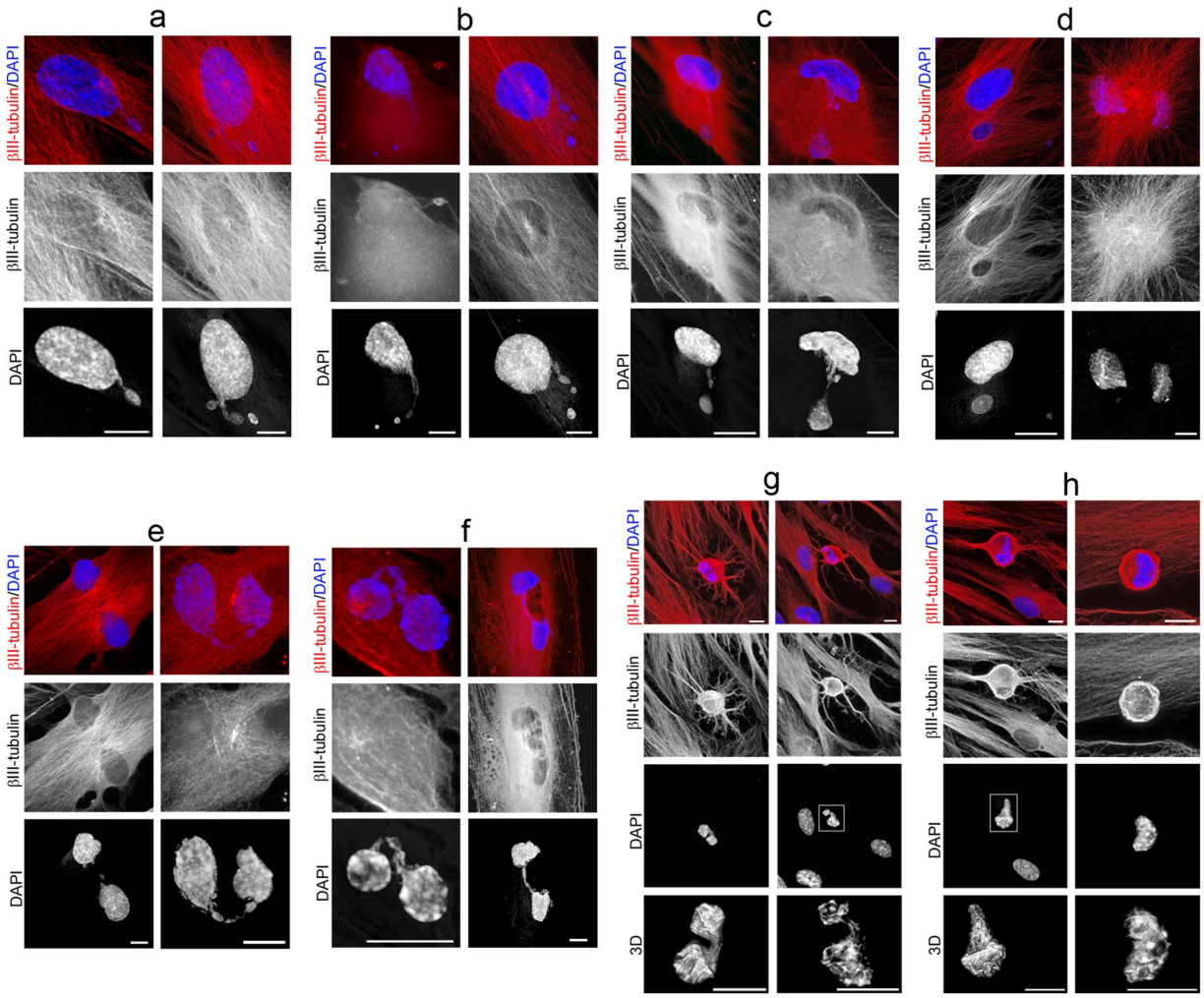

Figure 7. Nuclear shape remodeling occurs during neurogenesis from hPDLSCs. (**a**) Small DNA containing structures arise from the main nuclei and start to move (**b**) towards specific positions within the cell (**c**) and temporarily form lobed nuclei (**d**). Later, these lobed nuclei connected to one another through small DNA containing structures (**e**) forming nucleoplasmic bridges (**f**). Finally, lobed nuclei connected by an internuclear bridge (**g**) join in a single nucleus with an eccentric position within hPDLSCs-derived neural-like cells (**h**). The scale bars in β-III tubulin and DAPI images are 50 μm and 10 μm for confocal 3D images of nuclei.

Interestingly, the morphological analysis revealed that the adult rodent V-SVZ of the anterolateral ventricle wall (Fig. 8a) and the SGZ of the hippocampal dentate gyrus (Fig. 8b), where adult neurogenesis has been clearly demonstrated, contained cells with nuclear shapes highly similar to those observed during *in vitro* neurogenesis from hPDLSCs.

It is important to mention that nuclear morphology of hPDLSCs observed during *in vitro* neurogenesis from hPDLSCs (Fig. 7) are highly similar to nuclear morphology of V-SVZ B cells in the human fetal brain[42] and V-SVZ B cells in adult mice brain[43–45]. Although it has been suggested that lobed nuclei connected by an internuclear bridge are associated with quiescence in aNSCs[45], we observed that this kind of nuclei may be associated to nuclear movement within the cell during initial phases of neurogenesis, without being related to cell proliferation.

Discussion

In this study we show that hPDLSCs-derived neural-like cells display stages of development highly similar to those reported before in primary neuronal cultures derived from rodent brains[1,2,5,6]. The hPDLSCs-derived neural-like cells gradually adopted a complex morphology by forming several processes, that grew and arborized, adquiring dendritic-like and axonal-like identities, giving rise to a variety of neuron-like morphologies.

During neuronal polarization *in vivo*, the stages of development observed in mouse immature neurons are not necessarily the same as those observed *in vitro*, since they depend on the stage of development and the brain region[1,2]. In a previous publication, we showed that hPDLSCs-derived neural-like cells integrate and differentiate after implantation into the adult mammalian brain[18]. It is important to mention that the hPDLSCs-derived neural-like cells located in the NSC niches show neural stem morphology, which suggests hPDLSCs-derived neural-like cells may achieve a correct polarization *in vivo*.

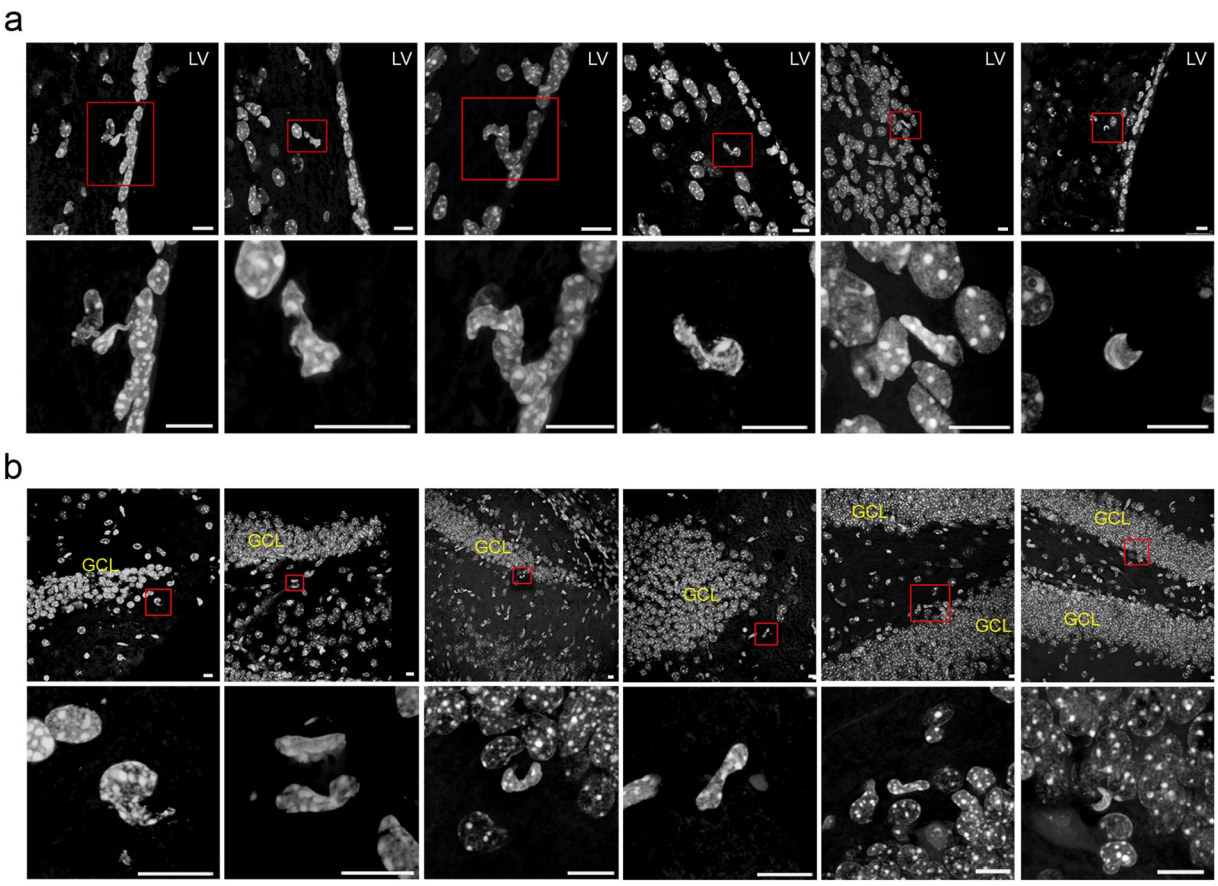

Figure 8. Neurogenic niches in the adult mammalian brain also contains cells with irregular nuclei. Morphological analysis reveals that the adult rodent V-SVZ of the anterolateral ventricle wall (**a**), as well as the SGZ of the hippocampal dentate gyrus (**b**), contain cells with nuclear shapes highly similar to those observed in during *in vitro* neurogenesis from hPDLSCs. Scale bar: 10 μm. GLC, granule cell layer; LV, lateral ventricle.

Therefore, our results provide additional evidence that it is possible to differentiate hPDLSCs to neuron-like cells, as suggested by their neural-crest origin, stem cell characteristics and neural differentiation potential both *in vitro* and *in vivo*[13–24]. However, it is important to mention that future research is required to resolve the potential limitations in their medical application[10,14,46], and also to optimize the diversity of *in vitro* neural induction protocols that have been designed for dental stem cells[22]. In addition, future analysis will be necessary to study neural linages derived from hPDLSCs including neuron-like, astrocyte-like, and oligodendrocyte-like cells.

In this study, we also show that cell proliferation is not present through neurogenesis from hPDLSCs. The undifferentiated polygonal and fusiform cell shapes are reset and start their neuronal development as round spheres. As noted above, morphological characteristics of the hPDLSCs, including cytoskeleton and nuclear morphology were examined in cells under proliferation and neural differentiation conditions.

During mitosis, the nucleolus and the nuclear lamina are reversibly disassembled and β-III tubulin protein is present in the mitotic spindle and it is detectable in all phases of mitosis. Moreover, mitotic chromosomes and cytokinesis were observed. Mitosis and cytokinesis last no more than 2 hours. During neurogenesis, the nucleolus and the nuclear lamina are not disassembled, contrary to what happens during mitosis[39,40]. Moreover, mitotic chromosomes, mitotic spindle and cytokinesis were not observed. In addition, the duration of the morphological changes that occurred when the hPDLSCs round up to a near-spherical shape lasts much longer than mitosis and cytokinesis. Collectively, these results revealed that round cells do not represent dividing cells.

In this study, we may have discovered a transient cell nuclei lobulation coincident to *in vitro* neurogenesis. Ultrastructural analysis with transmission electron microscopy revealed that hPDLSCs with lobed nuclei do not represent apoptotic cells due to the absence of features of cells undergoing apoptotis[41]. Interestingly, the morphological analysis revealed that the adult rodent V-SVZ of the anterolateral ventricle wall and the SGZ of the hippocampal dentate gyrus contained cells with nuclear shapes highly similar to those observed during *in vitro* neurogenesis from hPDLSCs. It is important to mention that nuclear morphology of hPDLSCs observed during *in vitro* neurogenesis from hPDLSCs are highly similar to nuclear morphology of V-SVZ B cells in the human fetal brain[42] and V-SVZ B cells in adult mice brain[43–45].

The presence of neural stem cells in the adult mammalian brain (aNSCs) have been described in two neurogenic niches, the V-SVZ of the anterolateral ventricle wall and the subgranular zone SGZ of the hippocampal dentate gyrus[43,47–53]. The study of the cell composition of neurogenic niches and the use of methods for detecting

proliferating cells, suggest that neurogenesis occurs progressively through sequential phases of proliferation and the neuronal differentiation of aNSCs.

In the V-SVZ, putative aNSCs (type B cells) divide to give rise to intermediate progenitor cells (type C cells), which divide a few times before becoming neuroblasts (type A cells). The neuroblast then migrate into the olfactory bulb and differentiate into distinct types of neurons[43,48,49].

In the SGZ, putative aNSCs divide to give rise to intermediate progenitor cells which exhibit limited rounds of proliferation before generating polarized neuroblast[49–53]. Neuroblast, as polarized cells, then migrate, guided by the leading process, along SGZ and differentiate into dentate granule neurons[54,55].

Previous ultrastructure and immunocytochemistry studies show that the V-SVZ stem cell niche contains cells with different morphologies and irregular nuclei[42–45,47,48,56–58]. Type-B cells have irregular nuclei that frecuently contain invaginations and irregular contours of the plasma membrane. Type-C cells nuclei contained deep invaginations and these cells are more spherical. Type-A cells have elongated cell body with one or two processes and the nuclei are occasionally invaginated[43]. Importantly, some studies have shown that murine and human V-SVZ have segmented nuclei connected by an internuclear bridge[42,44,45]. Although it has been suggested that lobed nuclei connected by an internuclear bridge are associated with quiescence in aNSCs[45], we observed that this kind of nuclei may be associated to nuclear movement within the cell during initial phases of neurogenesis, without being related to cell proliferation.

In addition, previous reports also shown irregular shaped nuclei in the adult SGZ[59–66]. Adult SGZ NSCs (type 1 cells) have irregular contours of the plasma membrane, and differences in heterochromatin aggregation has been also observed[53]. Futhermore, adult SGZ NSCs (type 2 cells) had an irregularly shaped nucleus[55,67]. Importantly, one study also found that many cultured hippocampal neurons have irregular nuclei or even consisted of two or more lobes connected by an internuclear bridge[68].

It has commonly been assumed that adult neurogenesis occurs progressively through sequential phases of proliferation[54,55]. Despite the advantages for the detection of adult neurogenesis using exogenous nucleotide analog administration or endogenous cell cycle markers, in addition to retroviral transduction, cell stage and lineage commitment markers, recent findings indicate that some observations interpreted as cell division could be false-positive signals[69–72]. The main method used to labed new neurons has been the incorporation of the thymidine analogs into the genome of dividing cells during S-phase of the cell cycle, but nevertheless thymidine analogs such as tritiated thymidine, BrdU, CldU and IdU may also be incorporated during DNA turnover or DNA repair[69–72]. Infection with retrovirus is another method used to label new neurons however, retroviral vectors not specifically infect dividing cells[71] and also, it has even been observed that postmitotic pyramidal neurons can also be labeled by fused infected microglia[73]. Although the expression of endogenous cell cycle proteins is also used to label new neurons, recent findings indicate that cell cycle proteins expression is not necessarily related to cell division[72]. Proliferating cell nuclear antigen is also invoved in DNA repair[74]. Positivity of the proliferation marker KI-67 in noncycling cells has also been observed[75].

These findings indicate that there is a lack of a reliable definitive method to label new neurons. In addition, it is important to note that almost none of these labeled new born neurons show mitotic chromosomes or mitotic spindle to really confirm that adult neurogenesis occurs progressively through sequential phases of proliferation[43,47–53]. Importantly, the existence of non-proliferative neuronal precursors in several brain areas has also been observed[76,77]. Moreover, the self-renewal and multipotent properties demonstrated by NSC *in vitro*[78] have not been clearly demonstrated *in vivo*[54,67,79].

Collectively, these results suggest the possibility that the sequence of events from aNSCs to neuron may also occur without being related to cell proliferation. It would therefore be interesting to examine whether SVZ and SGZ intermediate progenitor cells represent different stages of neurogenesis without being related to cell proliferation.

It is known for many decades that adult cells can change their indentity throught spontaneous dedifferentiation, differentiation and transdiferentiation *in vitro* and *in vivo*[80–82]. Future analysis will be necessary to study if hPDLSCs convert directly to neural-like cells or if they go through neural progenitor stage first. Our results suggest the possibility that hPDLSCs could be use to advance knowledge of the cellular plasticity.

Beyond the central nervous system, the presence of lobed nuclei has been reported in most blood and immune cells, but the functional significance of multilobed nuclear structures is not yet known[83–86]. We observed that the nuclei of hPDLSCs during initial phases of neurogenesis are highly similar to those reported in immune cells. Thus, we suggest the possibility that multilobed nuclear structures may be associated to nuclear movement within the cell. Therefore, it would also be interesting to examine whether these putative madure cells also represent different stages of haematopoietic stem cell differentiation without being related to cell proliferation.

One of the most important discoveries in this work is the observation that small DNA containing structures may move within the cell to specific directions and temporarily form lobed nuclei. These small DNA containing structures displayed a spherical or ovoid shape, and it seems that some of them are connected to the main body of the nucleus by thin strands of nuclear material. It is important to note that some DNA containing structures are highly similar to nuclear envelope-limited chromatin sheets (ELCS)[45,87,88]. Fibrillarin and lamin A/C proteins were detected in these small DNA containing structures.

It is known for many decades that chromatin particles can appear in the cellular cytoplasm and they are referred to as micronuclei, nucleoplasmic bridge and nuclear bud[89]. Although these nuclear anomalies have been associated with chromosomal instability events during mitosis[89–92], recent reports showed generation of micronuclei during interphase[93–95]. These findings call into question that micronuclei, nucleoplasmic bridge and nuclear bud does necessarily generated during mitosis[96]. Moreover, a high frequency of human mesenquimal stem cells with nuclear bud, micronuclei and nucleoplasmic bridge was detected under normal *in vitro* culture[97]. Therefore, the mechanisms that lead to extra-nuclear bodies formation and their biological relevance are still far from been understood[96,98,99].

In this study, we show that there can be a relationship in the formation of the nuclear bud, micronuclei, nucleoplasmic bridge and nuclear envelope-limited chromatin sheets. Collectively, these results suggest the possibility that the interphase cell nucleus may can reversibly disassembled into functional subunits that may moved independently within the cell, if necessary.

Multinuclear cells are commonly found in various human organs including heart, liver, salivary glands, muscle and endometrium, but their functional advantage remains unknown[100,101]. In addition, alterations in nuclear morphologies are closely associated with a wide range of human diseases, including cancer[102]. hPDLSCs could facilitate an understanding of the mechanisms regulating nuclear morphology in response to cell shape changes and their functional relevance[103,104].

Methods

Ethical conduct of research. Methods were carried out in accordance with the relevant guidelines and regulations. The experimental protocols were approved by the Institutional Review Board of the Miguel Hernández University of Elche (No. UMH.IN.SM.03.16) and the signed informed consent was obtained from all patients before the study. The authors declare that all experiments on human subjects were conducted in accordance with the Declaration of Helsinki. All protocols and care of the mice were carried out according to the guidelines of the European Communities Council Directive of 24 November 1986 (86/609/EEC). The authors further attest that all efforts were made to minimize the number of animals used and their suffering.

Cell culture. Dissociated cell cultures of hPDL tissue were prepared as previously described[18]. Human premolars were extracted and collected from three different healthy adult donors undergoing orthodontic therapy in Murcia dental hospital (Spain). hPDL was scraped from the middle third region of the root surface. After washing the extracted PDL with Ca and Mg-free Hank's balance salt solution (HBSS; Gibco), hPDL was digested with 3 mg/ml type I collagenase (Worthington Biochemical Corporation) and 4 mg/ml dispase II (Gibco) in alpha modification minimum essential medium eagle (α-MEM) (α-MEM; Sigma-Aldrich) for 1 h at 37 °C. The reaction was stopped by the addition of α-MEM. PDL derived from different subjects were pooled together to obtain single cell suspensions by passing the cells through a 70 μm strainer (BD Falcon). Cells were centrifuged, and the pellet was resuspended in in serum-containing media (designated as the basal media), composed of α-MEM supplemented with 15% calf serum (Sigma), 100 units/ml penicillin-streptomycin (Sigma) and 2 mM l-glutamine (Sigma). The cell suspension was plated into six-well multiwell plates (BD Falcon) and incubated at 37 °C in 5% CO_2. The cells at passage 3–4 were then used for the following experiments. We used μ-Dish 35 mm, high Grid-500 (Ibidi) for live cell imaging. Numeric marks on the bottom of each dish allow users to identify the location of cells.

To induce neural differentiation, cells were cultured in serum-free media (designated as the neural induction media), consisting in Dulbecco's modified Eagle's medium/F12 (DMEM/F12, Gibco) supplemented with bFGF (20 ng/ml, R&D Systems), EGF (20 ng/ml, R&D Systems), glucose (0.8 mg/ml, Sigma), N2-supplement (Gibco), 2 mM l-glutamine (Sigma), and 100 units/ml penicillin-streptomycin (Sigma). Cells at passage 3–4 were allowed to adhere to the plates overnight. Media was removed the following day and neural induction media was added directly to the cells. Neural induction media were changed every 3 days until the end of the experiment (2 weeks).

In previous publication[18], we showed that several stem cell and neural crest cell markers are expressed in human adult periodontal ligament (hPDL) tissue and hPDL-derived cells.

Immunocytochemistry. A standard immunocytochemical protocol was used as previously described[18]. Cells were plated onto collagen IV (Sigma) coated plastic or glass coverslips, and maintained in basal media or neural induction media. Cells were rinsed with PBS and fixed in freshly prepared 4% paraformaldehyde (PFA; Sigma). Fixed cells were blocked for 1 h in PBS containing 10% normal horse serum (Gibco) and 0.25% Triton X-100 (Sigma) and incubated overnight at 4 °C with antibodies against: β-III-tubulin (TUJ1; 1:500, Covance), Tau (GTX49353; 1/300, GeneTex), MAP2 (840601; 1/300, Biolegend), Connexin-43 (3512; 1/300, Cell Signalling), Synaptophysin (18-0130; 1/300, Zymed), Synapsin1 (NB300-104; 1/300, Novus), Fibrillarin (ab5821; 1/300, Abcam) and Lamin A/C (GTX101127; 1/300, GeneTex) in PBS containing 1% normal horse serum and 0.25% Triton X-100. On the next day, cells were rinsed and incubated with the corresponding secondary antibodies: Alexa Fluor® 488 (anti-mouse or anti-rabbit; 1:500, Molecular Probes), Alexa Fluor® 594 (anti-mouse or anti-rabbit; 1:500, Molecular Probes), biotinylated anti-rabbit (BA1000, 1:250; Vector Laboratories), biotinylated anti-chicken (BA9010, 1:250, Vector Laboratories, CY3-streptavidin (1:500, GE Healthcare). Cell nuclei were counterstained with DAPI (0.2 mg/ml in PBS, Molecular Probes). Alexa Fluor 488® phalloidin was used to selectively stains F-actin (Molecular Probes). Data are representative of ten independent experiments per condition.

Western blotting. A standard Western Blott protocol was used as previously described[18]. hPDL-derived cells (in basal media) were harvested using trypsin/EDTA (Gibco), washed twice with PBS, resuspended in RIPA lysis buffer (Millipore) in the presence of protease inhibitors (Pierce™. protease inhibitor Mini Tables, Pierce Biotechnology Inc) and PMSF 1 M (Abcam) for 30 min at 4 °C. Protein concentration was determined using the bradford protein assay (Sigma-Aldrich). Proteins were separated in 8% SDS-polyacryamide gel (PAGE-SDS) and transferred to a nitrocellulose membrane (Whatman). PageRuler™ Prestained Protein Ladder (Thermo Scientific) has been used as size standards in protein electrophoresis (SDS-PAGE) and Western-Blotting. After transfer, nitrocellulose membranes were stained with Ponceau S solution (Sigma-Aldrich) to visualize protein bands. Blots were then incubated over-night at 4 °C with rabbit antibody against β-III-tubulin (TUJ1; 1:1000, Covance). Secondary antibody was used at 1:7000 for peroxidase anti-mouse Ab (PI-2000, Vector Laboratories). Immunoreactivity was detected using the enhanced chemiluminescence (ECL) Western blot detection system

(Amersham Biosciences Europe) and Luminata™ Forte (Millipore corporation) using ImageQuant *LAS 500* Gel Documentation System (GE Healthcare). The molecular weight of β-III-tubulin is approximately 55 kDa.

Immunohistochemistry. A standard immunohistochemistry protocol was used as previously described[18]. Experiments were carried out according to the guidelines of the European Community (Directive 86/609/ECC) and in accordance with the Society for Neuroscience recommendations. Animals used in this study were 12-week-old immune-suppressed mouse (Hsd:Athymic Nude-Foxn1 nu/nu; Harlan Laboratories Models, S.L), housed in a temperature and humidity controlled room, under a 12 h light/dark cycles, with *ad libitum* access to food and water. The animals were anesthetized and intracardially perfused with freshly prepared, buffered 4% PFA (in 0.1 M PB, pH 7.4). Brains were removed, post-fixed for 12 hr in the same fixative at 4 °C and dehydrated in 30% sucrose solution at 4 °C until sunk. 30 µm thick coronal sections were collected using a freezing microtome. Serial sections were used for DAPI staining. Free-floating sections were incubated and mounted onto Superfrost Plus glass slides (Thermo Scientific). The slides were dried O/N and coverslipped with mowiol-NPG (Calbiochem).

Images and data analyses. Analyses and photography of visible and fluorescent stained samples were carried out in an inverted Leica DM IRB microscope equipped with a digital camera Leica DFC350FX (Nussloch) or in confocal laser scanning microscope Leica TCS-SP8. Digitized images were analyzed using LASX Leica confocal software. Z-stacks of confocal fluorescent images were also analyzed to calculate the nuclear volume by using ImageJ software.

We used Photoshop software to improve the visibility of fluorescence images without altering the underlying data. The fluorescent photographs presented in this study are original fluorescence images and inverted images (negatives) that are produced from the original fluorescence images.

Scanning electron microscopy. Cells were plated onto collagen IV (Sigma) coated glass coverslips and maintained in basal media or neural induction media. Cells were treated with fixative for 20 minutes. Coverslips were postfixed in 1% osmium tetroxide for 1 hour and dehydrated in graded ethanol washes. The coverslips were allowed to dry at a conventional critical point and were then coated with gold-palladium sputter coated. Coverslips were view on a Jeol 6100 scanning electron microscope.

Transmission electron microscopy. hPDL-derived cells were harvested using trypsin/EDTA (Gibco) and were treated with fixative for 60 minutes. Cells were postfixed in osmium tetroxide solution, dehydrated embedded in resin. Ultrathin sections (70–90 nm) were cut, stained with lead citrate, and examined under Jeol 1011 and Philips Tecnai 12 transmission electron microscopes.

Received: 2 August 2019; Accepted: 15 November 2019;
Published online: 02 December 2019

References

1. Tahirovic, S. & Bradke, F. Neuronal polarity. *Cold Spring Harb. Perspect. Biol.* **1**, a001644, https://doi.org/10.1101/cshperspect.a001644 (2009).
2. Takano, T., Xu, C., Funahashi, Y., Namba, T. & Kaibuchi, K. Neuronal polarization. *Development.* **142**, 2088–2093 (2015).
3. Schelski, M. & Bradke, F. Neuronal polarization: From spatiotemporal signaling to cytoskeletal dynamics. *Mol. Cell Neurosci.* **84**, 11–28 (2017).
4. Kaplan, A., Bueno, M., Hua, L. & Fournier, A. E. Maximizing functional axon repair in the injured central nervous system: Lessons from neuronal development. *Dev. Dyn.* **247**, 18–23 (2018).
5. Dotti, C. G., Sullivan, C. A. & Banker, G. A. The establishment of polarity by hippocampal neurons in culture. *J. Neurosci.* **8**, 1454–1468 (1988).
6. Powell, S. K., Rivas, R. J., Rodriguez-Boulan, E. & Hatten, M. E. Development of polarity in cerebellar granule neurons. *J. Neurobiol.* **32**, 223–236 (1997).
7. Ohara, Y. *et al*. Early-stage development of human induced pluripotent stem cell-derived neurons. *J. Neurosci. Res.* **93**, 1804–1813 (2015).
8. Azari, H. & Reynolds, B. A. *In vitro* models for neurogenesis. *Cold Spring Harb. Perspect. Biol.* **8**, a021279, https://doi.org/10.1101/cshperspect.a021279 (2016).
9. Conti, L. & Cattaneo, E. Neural stem cell systems: physiological players or *in vitro* entities? *Nat. Rev. Neurosci.* **11**, 176–187 (2010).
10. Casarosa, S., Bozzi, Y. & Conti, L. Neural stem cells: ready for therapeutic applications? *Mol. Cell Ther.*, **2**, https://doi.org/10.1186/2052-8426-2-31 (2014).
11. Goldman, S. A. Stem and progenitor cell-based therapy of the central nervous system: hopes, hype, and wishful thinking. *Cell Stem Cell.* **18**, 174–188 (2016).
12. Bronner-Fraser, M. Origins and developmental potential of the neural crest. *Exp. Cell Res.* **218**, 405–417 (1995).
13. Crane, J. F. & Trainor, P. A. Neural crest stem and progenitor cells. *Annu. Rev. Cell Dev. Biol.* **22**, 267–286 (2006).
14. Achilleos, A. & Trainor, P. A. Neural crest stem cells: discovery, properties and potential for therapy. *Cell Res.* **22**, 288–304 (2012).
15. Liu, J. A. & Cheung, M. Neural crest stem cell and their potential therapeutic applications. *Dev. Biol.* **419**, 199–216 (2016).
16. Seo, B. M. *et al*. Investigation of multipotent postnatal stem cells from human periodontal ligament. *Lancet* **364**, 149–155 (2004).
17. Tomokiyo, A. *et al*. Detection, Characterization, and Clinical Application of Mesenchymal Stem Cells in Periodontal Ligament Tissue. *Stem Cells Int.* **26**, 5450768, https://doi.org/10.1155/2018/5450768 (2018).
18. Bueno, C. *et al*. Human adult periodontal ligament-derived cells integrate and differentiate after implantation into the adult mammalian brain. *Cell Transplant.* **22**, 2017–2028 (2013).
19. Chiricosta, L., Diomede, F., Trubiani, O., Bramanti, P. & Mazzon, E. Physiological Expression of Ion Channel Receptors in Human Periodontal Ligament Stem Cells. *Cells.* **8**, E219, https://doi.org/10.3390/cells8030219 (2019).
20. Fortino, V. R., Chen, R. S., Pelaez, D. & Cheung, H. S. Neurogenesis of neural crest-derived periodontal ligament stem cells by EGF and bFGF. *J. Cell Physiol.* **229**, 479–488 (2014).
21. Ng, T. K. *et al*. Transdifferentiation of periodontal ligament-derived stem cells into retinal ganglion-like cells and its microRNA signature. *Sci. Rep.* **5**, 16429, https://doi.org/10.1038/srep16429 (2015).

22. Heng, B. C., Lim, L. W., Wu, W. & Zhang, C. An Overview of Protocols for the Neural Induction of Dental and Oral Stem Cells *In Vitro*. *Tissue Eng. Part B Rev.* **22**, 220–250 (2016).
23. Trubiani, O. *et al*. Nuclear translocation of PKCα isoenzyme is involved in neurogenic commitment of human neural crest-derived periodontal ligament stem cells. *Cell Signal.* **28**, 1631–1641 (2016).
24. Ng, T. K. *et al*. MicroRNA-132 directs human periodontal ligament-derived neural crest stem cell neural differentiation. *J. Tissue Eng. Regen. Med.* **13**, 12–24 (2019).
25. Flynn, K. C. The cytoskeleton and neurite initiation. *BioArchitecture.* **3**, 86–109 (2013).
26. Foudah, D. *et al*. Expression of neural markers by undifferentiated mesenchymal-like stem cells from different sources. *J. Immunol. Res.* **2014**, 987678, https://doi.org/10.1155/2014/987678 (2014).
27. Jouhilahti, E. M., Peltonen, S. & Peltonen, J. Class III beta-tubulin is a component of the mitotic spindle in multiple cell types. *J. Histochem. Cytochem.* **56**, 1113–1119 (2008).
28. Sanger, J. W. & Sanger, J. M. Surface and shape changes during cell division. *Cell Tissue Res.* **209**, 177–186 (1980).
29. Sanger, J. M., Reingold, A. M. & Sanger, J. W. Cell surface changes during mitosis and cytokinesis of epithelial cells. *Cell Tissue Res.* **237**, 409–417 (1984).
30. Forscher, P. & Smith, S. J. Actions of Cytochalasins on the organization of actin filaments and microtubules in a neuronal growth cone. *J. Cell Biol.* **107**, 1505–1516 (1988).
31. Blanquie, O. & Bradke, F. Cytoskeleton dynamics in axon regeneration. *Curr. Opin. Neurobiol.* **51**, 60–69 (2018).
32. Ros, O., Cotrufo, T., Martinez-Marmol, R. & Soriano, E. Regulation of patterned Dynamics of local exocytosis in growth cone by netrin-1. *J. Neurosci.* **35**, 5156–5170 (2015).
33. Hering, H. & Sheng, M. Dendritic spines: Structure, dynamics and regulation. *Nature Rev. Neurosci.* **2**, 880–888 (2001).
34. Von Bohlen Und Halbach, O. Structure and functions of dendritic spines. *Ann. Anat.* **191**, 518–531 (2009).
35. Merriam, E. B. *et al*. Synaptic regulation of microtubule dynamics in dendritic spines by calcium, F-actin, and debrin. *J. Neurosci.* **33**, 164711–164782 (2013).
36. Gibson, D. A. & Ma, L. Developmental regulation of axon branching in the vertebrate nervous system. *Development.* **138**, 183–195 (2011).
37. Ochs, R. L., Lischwe, M. A., Spohn, W. H. & Busch, H. Fibrillarin: a new protein of the nucleolus identified by autoimmune sera. *Biol. Cell.* **54**, 123–133 (1985).
38. De Leeuw, R., Gruenbaum, Y. & Medalia, O. Nuclear Lamins: Thin Filaments with Major Functions. *Trends Cell Biol.* **28**, 34–45 (2018).
39. Rodriguez-Corona, U., Sobol, M., Rodriguez-Zapata, L. C., Hozak, P. & Castano, E. Fibrillarin from Archaea to human. *Biol. Cell.* **107**, 159–174 (2015).
40. Németh, A. & Grummt, I. Dynamic regulation of nucleolar architecture. *Curr. Opin. Cell Biol.* **52**, 105–111 (2018).
41. Elmore, S. Apoptosis: a review of programmed cell death. *Toxicol Pathol.* **35**, 495–516 (2007).
42. Guerrero-Cázares, H. *et al*. Cytoarchitecture of the lateral ganglionic eminence and rostral extension of the lateral ventricle in the human fetal brain. *J. Comp. Neurol.* **519**, 1165–1180 (2011).
43. Doetsch, F., Garcia-verdugo, J. M. & Alvarez-buylla, A. Cellular composition and three-dimensional organization of the subventricular germinal zone in the adult mammalian brain. *J. Neurosci.* **17**, 5046–5061 (1997).
44. Capilla-Gonzalez, V., Cebrian-Silla, A., Guerrero-Cazares, H., Garcia-Verdugo, J. M. & Quiñones-Hinojosa, A. Age-related changes in astrocytic and ependymal cells of the subventricular zone. *Glia.* **62**, 790–803 (2014).
45. Cebrián-Silla, A. *et al*. Unique organization of the nuclear envelope in the post-natal quiescent neural stem cells. *Stem Cell Reports.* **9**, 203–216 (2017).
46. Wang, Y., Han, Z. B., Song, Y. P. & Han, Z. C. Safety of mesenchymal stem cells for clinical application. *Stem Cells Int.* **2012**, 652034, https://doi.org/10.1155/2012/652034 (2012).
47. Doetsch, F., Garcia-verdugo, J. M. & Alvarez-buylla, A. Regeneration of a germinal layer in the adult mammalian brain. *Proc. Natl. Acad. Sci.* **96**, 11619–11624 (1999).
48. Doetsch, F., Caillé, I., Garcia-verdugo, J. M. & Alvarez-buylla, A. Subventricular zone astrocytes are neural stem cells in the adult mammalian brain. *Cell.* **97**, 703–716 (1999).
49. Seri, B., Garcia-verdugo, J. M., McEwen, B. S. & Alvarez-buylla, A. Astrocytes give rise to new neurons in the adult mammalian hippocampus. *J. Neurosci.* **21**, 7153–7160 (2001).
50. Filippov, V. *et al*. Subpopulation of nestin-expressing progenitor cells in the adult murine hippocampus shows electrophysiological and morphological characteristics of astrocytes. *Mol. Cell Neurosci.* **23**, 373–382 (2003).
51. Kronenberg, G. *et al*. Subpopulations of proliferating cells of the adult hippocampus respond differently to physiologic neurogenic stimuli. *J. Comp. Neurol.* **467**, 455–463 (2003).
52. Seri, B., Garcia-verdugo, J. M., Collado-Morente, L., McEwen, B. S. & Alvarez-buylla, A. Cell types, lineage, and architecture of the germinal zone in the adult dentate gyrus. *J. Comp. Neurol.* **474**, 359–378 (2004).
53. Kempermann, G., Jessberger, S., Steiner, B. & Kronenberg, G. Milestones of neuronal development in the adult hippocampus. *Trends Neurosci.* **27**, 447–452 (2004).
54. Bond, A. M., Ming, G. L. & Song, H. Adult mammalian neural stem cells and neurogenesis: five decades later. *Cell Stem Cell.* **17**, 385–395 (2015).
55. Fuentealba, L. C., Obernier, K. & Alvarez-Buylla, A. Adult stem cells bridge their niche. *Cell Stem Cell.* **10**, 678–708 (2012).
56. Smart, I. The subependymal layer of the mouse brain and its cell production as shown by radioautography after thymidine-H3 injection. *J. Com. Neurol.* **116**, 325–347 (1961).
57. Privat, A. & Leblond, C. P. The subependymal layer and neighboring region in the brain of the young rat. *J. Com. Neurol.* **146**, 277–302 (1972).
58. Sturrock, R. R. & Smart, I. H. A morphological study of the mouse subependymal layer from embryonic life to old age. *J. Anat. Mar.* **130**, 391–415 (1980).
59. Ribak, C. E. & Anderson, L. Ultrastructure of the pyramidal basket cells in the dentate gyrus of the rat. *J. Comp. Neurol.* **192**, 903–916 (1980).
60. Ribak, C. E. & Seress, L. Five types of basket cell in the hippocampal dentate gyrus: a combined Golgi and electron microscopic study. *J. Neurocytol.* **12**, 577–597 (1983).
61. Kaplan, M. S. & Bell, D. H. Mitotic neuroblasts in the 9-day-old and 11-month-old rodent hippocampus. *J. Neurosci.* **4**, 1429–1441 (1984).
62. Seress, L. & Ribak, C. E. A combined Golgi-electron microscopic study of non-pyramidal neurons in the CA 1 area of the hippocampus. *J. Neurocytol.* **14**, 717–730 (1985).
63. Seki, T. & Arai, Y. Highly polysialylated neural cell adhesion molecule (NCAM-H) is expressed by newly generated granule cells in the dentate gyrus of the adult rat. *J. Neurosci.* **13**, 2351–2358 (1993).
64. Kuhn, H. G., Dickinson-Anson, H. & Gage, F. H. Neurogenesis in the dentate gyrus of the adult rat: Age-Related decrease of neuronal progenitor proliferation. *J. Neurosci.* **16**, 2027–2033 (1996).
65. Parent, J. M. *et al*. Dentate granule cell neurogenesis is increased by seizures and contributes to aberrant network reorganization in the adult rat hippocampus. *J. Neurosci.* **17**, 3727–3738 (1997).

66. Urbach, A., Redecker, C. & Witte, O. W. Induction of neurogenesis in the adult dentate gyrus by cortical spreading depression. *Stroke.* **39**, 3064–3072 (2008).
67. Gabay, L., Lowell, S., Rubin, L. L. & Anderson, D. J. Deregulation of dorsoventral patterning by FGF confers trilineage differentiation capacity on CNS stem cells *in vitro*. *Neuron.* **40**, 485–499 (2003).
68. Wittmann, M. *et al*. Synaptic activity induces dramatic changes in the geometry of the cell nucleus: interplay between nuclear structure, histone H3 phosphorylation, and nuclear calcium signaling. *J. Neurosci.* **29**, 14687–14700 (2009).
69. Rakic, P. Adult neurogenesis in mammals: an identity crisis. *J. Neurosci.* **22**, 614–618 (2002).
70. Cooper-Kuhn, C. M. & Kuhn, H. G. Is it all DNA repair? Methodological considerations for detecting neurogenesis in the adult brain. *Brain Res. Dev.* **134**, 13–21 (2002).
71. Breunig, J. J., Arellano, J. I., Macklis, J. D. & Rakic, P. Everything that glitters isn't gold: a critical review of postnatal neural precursor analyses. *Cell Stem Cell.* **1**, 612–627 (2007).
72. Kuhn, H. G., Eisch, A. J., Spalding, K. & Peterson, D. A. Detection and Phenotypic Characterization of Adult. *Neurogenesis. Cold Spring Harb. Perspect. Biol.* **8**, a025981, https://doi.org/10.1101/cshperspect.a025981 (2016).
73. Ackman, J. B., Siddiqi, F., Walikonis, R. S. & LoTurco, J. J. Fusion of Microglia with Pyramidal Neurons after Retroviral Infection. *J. Neurosci.* **26**, 11413–11422 (2006).
74. Uberti, D., Ferrar-Toninelli, G. & Memo, M. Involvement of DNA damage and repair systems in neurodegenerative process. *Oxico. L. Lett.* **139**, 99–105 (2003).
75. Van Oijen, M. G., Medema, R. H., Slootweg, P. J. & Rijksen, G. Positivity of the proliferation marker Ki-67 in noncycling cells. *Am. J. Clin. Pathol.* **110**, 24–31 (1998).
76. König, R. *et al*. Distribution and fate of DCX/PSA-NCAM expressing cells in the adult mammalian cortex: a local reservoir for adult cortical neuroplasticity? *Front. Biol.* **11**, 193–213 (2016).
77. Rotheneichner, P. *et al*. Cellular Plasticity in the Adult Murine Piriform Cortex: Continuous Maturation of Dormant Precursors Into Excitatory Neurons. *Cereb. Cortex.* **28**, 2610–2621 (2018).
78. Reynolds, B. A. & Weiss, S. Generation of neurons and astrocytes from isolated cells of the adult mammalian central nervous system. *Science.* **255**, 1707–1710 (1992).
79. Suh, H. *et al*. *In vivo* fate analysis reveals the multipotent and self-renewal capacities of Sox2+ neural stem cells in the adult hippocampus. *Cell Stem Cell.* **1**, 515–528 (2007).
80. Raff, M. Adult stem cell plasticity: fact or artifact? *Annu. Rev. Cell Dev. Biol.* **19**, 1–22 (2003).
81. Tata, P. R. & Rajagopal, J. Cellular plasticity: 1712 to the present day. *Curr. Opin. Cell Biol.* **43**, 46–54 (2016).
82. Merrell, A. J. & Stanger, B. Z. Adult cell plasticity *in vivo*: de-differentiation and transdifferentiation are back in style. *Nat. Rev. Mol. Cell Biol.* **17**, 413–25 (2016).
83. Hoffmann, K., Sperling, K., Olins, A. L. & Olins, D. E. The granulocyte nucleus and lamin B receptor: avoiding the ovoid. *Chromosoma.* **116**, 227–235 (2007).
84. Carvalho, L. O., Aquino, E. N., Neves, A. C. & Fontes, W. The neutrophil nucleus and its role in neutrophilic function. *J. Cell Biochem.* **116**, 1831–1836 (2015).
85. Skinner, B. M. & Johnson, E. E. Nuclear morphologies: their diversity and functional relevance. *Chromosoma.* **126**, 195–212 (2017).
86. Georgopoulos, K. In search of the mechanism that shapes the neutrophil´s nucleus. *Genes Dev.* **31**, 85–87 (2017).
87. Olins, D. E. & Olins, A. L. Nuclear envelope-limited chromatin sheets (ELCS) and heterochromatin higher order structure. *Chromosoma.* **118**, 537–548 (2009).
88. Eltsov, M., Sosnovski, S., Olins, A. L. & Olins, D. E. ELCS in ice: cryo-electron microscopy of nuclear envelope-limited chromatin sheets. *Chromosoma.* **123**, 303–312 (2014).
89. Fenech, M. *et al*. Molecular mechanisms of micronucleus, nucleoplasmic bridge and nuclear bud formation in mammalian and human cells. *Mutagenesis.* **26**, 125–132 (2011).
90. Hutchison, H. E. & Ferguson-Smith, M. A. The significance of Howell-Jolly bodies in red cell precursors. *J. Clin. Pathol.* **12**, 451–53 (1959).
91. Dawson, D. W. & Bury, H. P. The significance of Howell-Jolly bodies and giant metamyelocytes in marrow smears. *J. Clin. Pathol.* **14**, 374–380 (1961).
92. Heddle, J. A. & Carrano, A. V. The DNA content of micronuclei induced in mouse bone marrow by gamma-irradiation: evidence that micronuclei arise from acentric chromosomal fragments. *Mutat. Res.* **44**, 63–69 (1977).
93. Shimizu, N., Itoh, N., Utiyama, H. & Wahl, G. M. Selective entrapment of extrachromosomally amplified DNA by nuclear budding and micronucleation during S phase. *J. Cell Biol.* **140**, 1307–1320 (1998).
94. Haaf, T. *et al*. Sequestration of mammalian Rad51-recombination protein into micronuclei. *J. Cell Biol.* **144**, 11–20 (1999).
95. Utani, K., Okamoto, A. & Shimizu, N. Generation of micronuclei during interphase by coupling between cytoplasmic membrane blebbing and nuclear budding. *PLoS One.* **6**, e27233, https://doi.org/10.1371/journal.pone.0027233 (2011).
96. Guo, X. *et al*. The molecular origins and pathophysiological consequences of micronuclei: New insights into an age-old problem. *Mutat. Res.* **779**, 1–35 (2019).
97. Cornélio, D. A., Tavares, J. C., Pimentel, T. V., Cavalcanti, G. B. & Batistuzzo de Medeiros, S. R. Cytokinesis-block micronucleus assay adapted for analyzing genomic instability of human mesenchymal stem cells. *Stem Cells Dev.* **23**, 823–838 (2014).
98. Hintzsche, H. *et al*. Fate of micronuclei and micronucleated cells. *Mutat Res.* **771**, 85–98 (2017).
99. Norppa, H. & Falck, G. C. What do human micronuclei contain? *Mutagenesis.* **18**, 221–233 (2003).
100. Miko, M. *et al*. Two nuclei inside a single cardiac muscle cell. *More questions than answers about the binucleation of cardiomyocytes. Biologia.* **72**, 825–830 (2017).
101. Manhart, A., Windner, S., Baylies, M. & Mogilner, A. Mechanical positioning of multiple nuclei in muscle cells. *PLoS Comput. Biol.*, **14**, e1006208, https://doi.org/10.1371/journal.pcbi.1006208, eCollection (2018)
102. Zink, D., Fischer, A. H. & Nickerson, J. A. Nuclear structure in cancer cells. *Nat. Rev. Cancer.* **4**, 677–687 (2004).
103. Gundersen, G. G. & Worman, H. J. Nuclear positioning. *Cell.* **152**, 1376–1389 (2013).
104. Dupin, I. & Etienne-Manneville, S. Nuclear positioning: mechanisms and functions. *Int. J. Biochem. Cell Biol.* **43**, 1698–1707 (2011).

Acknowledgements

We greatly appreciate the technical assistance of Microscopy Section of the University of Murcia in preparing samples for scanning electron microscopy and transmission electron microscopy. This work was supported by the grants Institute of Health Carlos III (RD16/001/0010) and Spanish MICINN (SAF2014-59347-C2-1-R) and (SAF2017-83702-R).

Author contributions

C.B. conceived of the study, designed the study, carried out the molecular lab work and drafted the manuscript. M.M. carried out the molecular lab work and participated in data analysis. S.M. conceived of the study, helped draft the manuscript and financial support. All authors discussed and commented on the manuscript.

Competing interests
The authors declare no competing interests.

Additional information
Supplementary information is available for this paper at https://doi.org/10.1038/s41598-019-54745-3.

Correspondence and requests for materials should be addressed to C.B.

Reprints and permissions information is available at www.nature.com/reprints.

Publisher's note Springer Nature remains neutral with regard to jurisdictional claims in published maps and institutional affiliations.